Orientation Development during Shear Flow-Induced Crystallization of i-PP

Florentin Langouche†

Solvay Central Laboratory, Neder Over Heembeek, Rue de Ransbeek 310, Brussels 1120, Belgium

Received December 1, 2005; Revised Manuscript Received February 3, 2006

ABSTRACT: Shear enhanced isothermal crystallization of i-PP was studied using a newly developed sandwich type shear cell and an optical setup with a modulated spinning laser. Considering a limited set of conditions, one temperature (140 °C) and one shear strain (100 units), we illustrate how this setup enables the characterization of the orientation development in homogeneous samples from the low shear rate region with spherulitic structures up into the highly oriented regime with row nucleated structure. At the same time, our choice of sample thickness allows us to measure the evolution of transmitted intensity. Further study of these features holds promise of a better characterization of the morphology development using optical techniques.

1. Introduction

Considerable experimental work has been done over the past few decades to reveal the mechanisms of morphological development during stress induced crystallization. It is now well established that even relatively low shear rates in the supercooled liquid can increase substantially the number of nuclei and therefore enhance the overall crystallization kinetics. On the basis of experimental determinations, scaling laws for the number of nuclei as a function of mechanical parameters and laws for characteristic crystallization times as a function of shear rates or shear stresses have been proposed.[1−3] Many results have been obtained in the low shear rate region,[4,5] and most of these results are obtained using either rheometrical equipment or using commercial shear cells like the Linkam CSS-450 shear cell. At higher shear rates, the issues of highly oriented layers which are present in the outer layers of injection molded specimens come up. However, experimental results extending into this highly oriented region are much more limited. The main results that have been published so far in this second region required specially designed extrusion dies, optical and on line X-ray detection techniques.[1,3] One important issue that has to be addressed as well in this region is the coupling between flow and the growing crystallites. For both regimes, the isothermal shear pulse protocol at relatively low undercooling pioneered by the group at the University of Linz with the aim of minimizing this coupling appears to be the most judicious procedure.

The relevancy to industrial processing is the challenge to predict microstructural details and mechanical part behavior, like stability, strength, and dimensional accuracy since mechanical properties of all layers will play a role in the final properties and the quality of the injection molded part. As a first step toward a prediction of the morphology a theory of shear induced crystallization is required. We tend to agree with recent comments of Janeschitz Kriegl[6] that an adequate modeling requires a sound physical picture of the underlying phenomena, a situation which has not yet been reached today even though several models have emerged[7−9] and some even have been implemented in commercial software.

Sound models have to be validated by experimental determination of the relevant parameters. The best strategy to characterize different products and to obtain the required parameters is still unknown. It is in this context that we present some new results obtained on an isotactic PP that seem promising. In our lab, we developed a sandwich type shear cell that can be operated from the low shear rate region up to the rates that generate the highly oriented structure. Its main advantage is that the structure probed by the optical technique is homogeneous and we will present below some new and interesting features of these measurements.

2. Experimental Section

Shear Cell. Our instrument is a small sandwich type cell in which the sample is uniaxially sheared between two oppositely moving glass windows, driven by a servomotor. The typical thickness of a sheared sample is 50−100 μm. Deformations up to a few hundred shear units can thus be achieved, which is typically what is realized in the outer layers during injection molding. The existence of a stationary plane in our flow field is useful for the optical observations. The unit is sufficiently rigid to withstand the normal forces generated within even highly viscous polymers. The use of a uniaxial shear cell is of course not new. In one of the first important studies in this field, Lagasse and Maxwell[10] had already used a stress (weight) controlled uniaxial cell to study crystallization. The windows of our cell are incorporated in sample holders which are located in moving conditioning blocks. Both conditioning blocks are independently heated using circulating oil baths and PT100 controllers. A precision on the order of 0.1 °C is therefore readily achieved.

To avoid the long cooling times typical of the extrusion die configurations that have been developed and have been used up to now in the literature, we decided to preheat the samples in a specially designed separate oven and to cool them to the measurement temperature by inserting them in the conditioning blocks. For isothermal measurements, the oil of the conditioning blocks therefore always remains at the same temperature and the thermal characteristics are such that a quenching time to the measurement temperature of a few minutes can be achieved for the sample. For isothermal measurements this leads to average cooling rates of 20−30 °C/min, comparable to the cooling characteristics of the Linkam cell.

We have chosen 140 °C as the measurement temperature for our i-PP sample that will be discussed. This choice of temperature has the advantage of a very slow quiescent crystallization time (>3 h). Moreover it is known that at this temperature crystallization proceeds mainly toward the α-phase.To erase the thermal prehistory we preheated the samples well above the equilibrium melting

† E-mail: Florentin.Langouche@solvay.com.

10.1021/ma0525684 CCC: $33.50
Published on Web 03/02/2006

temperature with a period of 5 min at 210 °C followed by a short preheating spike to 230 °C. Then we cool the samples to 190 °C before they are being transferred to the conditioning blocks kept at 140 °C. In practice the oil circulators are stopped for a short while and the conditioning blocks are allowed to cool a few degrees before inserting the sample holders. In this way we allow the heat loss to be compensated by the heat of the sample holders which leads to faster equilibration of the sample.

Optical Equipment. Windows and holes are provided in our equipment to view the flow-vorticity plane of the sheared sample along the flow gradient direction.

Preliminary measurements at low rates were performed with a white light source and a microscope using crossed polars at ±45° with respect to the flow direction. This optical setup was also used previously in our lab with a Linkam shearing hot stage and allowed us to determine the growth and nucleation rate characteristics of polymers by taking photographs of growing nuclei.

To follow the orientation at high shear rates, we modified our analysis technique. The structures formed in the high shear rate region are anyway so small that they cannot be resolved by optical microscopy.

We have installed a modulated spinning laser (the OAM module from TA Instruments) on the shear cell. The optical train of this instrument consists of a polarized diode laser beam at 670 nm, falling onto a spinning (∼400 Hz) half wave plate. Part of the beam is laterally deflected to a reference detector, the other part is transmitted trough the sample and analyzed by a circular analyzer and a photo detector. We added pinholes (1−1.5 mm) in front of the sample and the detector to improve the definition of the beam.

Apart from contributions related to the imperfection of the optical components, the signal in this setup gives a DC component and a $4\Omega t$ component for which we want to determine the amplitude. The intensity of the detected laser beam is given by[11]

$$I \approx I_o[1 + \sin(4\Omega t + 2\varphi)\sin\delta] \quad (1)$$

I_o is the initial intensity, Ω is the angular velocity of the spinner, and φ is the phase angle to be discussed below. In practice this signal is analyzed using a decomposition of the form

$$I = I_{DC} + I_{sin}\sin(4\Omega t) + I_{cos}\cos(4\Omega t)$$

where the phase is determined with respect to the detected reference signal $I = I_{ref}\sin(4\Omega t)$.

We connected both reference and sample signals from the OAM module to a data acquisition board in a PC and wrote appropriate software to achieve a temporal resolution of 2.5 ms (∼4 cycles/point) for the three components I_{DC}, I_{cos}, and I_{sin}. On-line analysis by emulating a lock-in amplifier would be possible, but our analysis simply treats the stored signal after the end of the measurement. The relevant physical information is extracted as

$$\mathrm{IDC/IDC}(t = 0)$$

giving the evolution of the transmitted intensity

$$|\sin\delta| = \frac{\sqrt{I_{sin}^{\ 2} + I_{cos}^{\ 2}}}{I_{DC}}$$

giving the birefringence.

Here $\delta = (2\pi e\Delta n'/\lambda)$, $\Delta n' = n'_{11} - n'_{22}$ is the birefringence in the 1−2 plane, λ(670 nm) is the laser wavelength and e is the sample thickness. In our computations we have systematically used the thickness as measured on the sample that is recovered after solidification.

During crystallization the experimental $|\sin(\delta)|$ term obtained using this procedure fails to go trough zero as shown in Figure 1.

The reason for this defect comes from dichroism, which can be independently measured by removing the circular polarizer. We observed it to be an order of magnitude smaller than the measured birefringence. Unfortunately, we cannot measure simultaneously

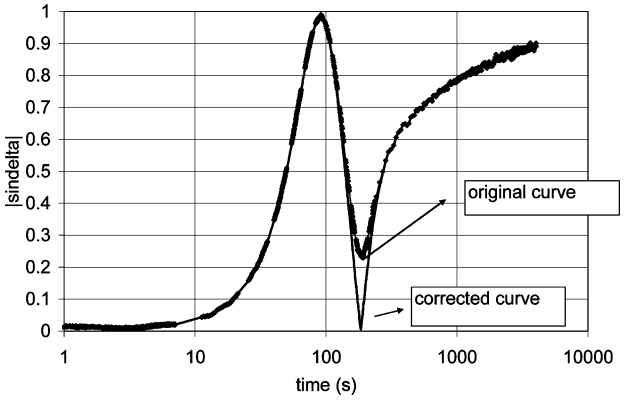

Figure 1. Example of birefringence development in a solidifying sample and of the correction applied to take into account the sample dichroism.

both contributions, but it turns out that there is an easy way around this problem. In fact, the setup gives not only the birefringence but also phase information (contained in the parameter φ of eq 1) related to reference angles and to the orientation of the principal axes. Using the knowledge of the orientation of the principal axes in the 1−2 plane (the flow and vorticity direction), we obtain directly some information on the dichroism.

In the presence of dichroism with principal axes parallel to the principal axes of birefringence, and oriented at an angle χ, we have according to ref 10

$$I = \frac{I_o}{2}[C + (-\cos 2\chi\cdot S + \sin 2\chi\cdot s)c_{4\theta} + (-\sin 2\chi\cdot S - \cos 2\chi\cdot s)s_{4\theta}]$$

where $c_{4\theta} = \cos(4\theta)$, $s_{4\theta} = \sin(4\theta)$, $C = \cosh(\delta'')$, $S = \sinh(\delta'')$, $s = \sin(\delta')$, and $c = \cos(\delta')$, with the usual relations between birefringence and retardation $\delta' = (2\pi e\Delta n')/\lambda$, and between dichroism and extinction $\delta'' = (2\pi e\Delta n'')/\lambda$.

The measured quantities are therefore

$$A \equiv \frac{\sqrt{I_{sin}^{\ 2} + I_{cos}^{\ 2}}}{I_{DC}} = \frac{\sqrt{S^2 + s^2}}{C} \quad \text{and}$$

$$B \equiv \frac{I_{sin}}{I_{cos}} = \frac{(-\sin 2\chi.S - \cos 2\chi.s)}{(-\cos 2\chi.S + \sin 2\chi.s)}$$

Using the shorthand notation A and B for both computed quantities, it is straightforward to solve for S and s

$$S = s\frac{(B\sin 2\chi + \cos 2\chi)}{(B\cos 2\chi - \sin 2\chi)} \equiv s\cdot Z$$

$$A^2 = \frac{S^2 + s^2}{1 + S^2} \quad \text{leading to} \quad s^2 = \frac{A^2}{1 - (A^2 - 1).Z^2}$$

In practice, this turns out to be sufficient to correct for the small dichroism effect in our experimental data. An example of the applied correction is shown in Figure 1.

Product. The polypropylene discussed in this publication is a Ziegler Natta injection molding grade. It concerns a former PP grade (HV252) from Solvay which corresponds to polymer A used in ref 4. This grade has a molecular weight of 181 kg/mol and a polydispersity of 7.3. The melt flow index (MFI) is 15. In the Supporting Information, we provide details of the dynamic and capillary viscosity for this grade at 200 °C. In light of current debates in the literature in which some authors investigate a pure melt rheological explanation for the creation of shish-kebab structures and the existence of a critical Deborah number for their creation, it seems important that our linear viscoelastic measurements extend to very low shear rates (10^{-3} rad/s) and effectively characterize the terminal relaxation time of the melt. Our experimental values of zero shear rate and steady-state compliance at

200 °C are $\eta_o = 2950$ Pa·s and $J^e_o = 10^{-3}$ (1/Pa). We hope that these details will be useful for theoretical considerations extending the work of ref 12 in order to characterize under the experimental conditions presented below the stretch of the longest molecules which are believed to form the shish of the oriented structures.

Shear Heating. The rheological data can also be used to examine if shear heating effects have to be considered during our experiments. From these data and time temperature superposition we can estimate the viscosity at the measurement temperature of 140 °C and at 1000 s^{-1} to be around 200 Pa·s. A shear pulse of 0.1 s would lead to an adiabatic heating of approximately 12 °C. A thermal (finite element) model of our shear cell shows that under these conditions the maximum temperature rise within a 100 μm film would only be 2.7 °C and would have dropped to 1.1 °C within 0.1 s and to 0.1 °C within 2 s. This is related to the fact that our shear layer is very thin and bounded by two surfaces. The maximal heating is critically dependent on the sample thickness. At 50 μm the maximum temperature rise during shear is limited to 1.2 °C and to 0.5 °C after 0.1 s. Since our conditions are intermediate, we should keep in mind a maximal shear heating of 2 °C during the shear pulse for the extreme shearing conditions, an effect which essentially has disappeared after 1 s.

3. Results

Measurement Example. All the measurements that are reported here correspond to approximately 100 units of applied shear. This seems to be a relevant choice since it captures the morphological transitions of the outer layers of injection molding specimens for our injection molding grade. From the practical point of view the conditions presented correspond to the optimal conditions of use of our instrument where we can be confident that the shear rate profile is boxlike and the programmed velocity is correctly imposed. These optimal conditions of use depend on sample thickness (temperature control, birefringence signal), velocity, and displacement considerations. To explore the ultimate limitations of the instrument, we are in the process of adding extra instrumentation to measure simultaneously the velocity profile. This will become relevant for much shorter shear pulses. In our results, the zero of the time scale corresponds to the start of the shear. Figure 2 shows a typical result obtained for $|\sin(\delta)|$ in a measurement at a shear rate of 600 s^{-1} during 0.2 s. We clearly distinguish the flow birefringence with a slight overshoot and stabilizing after 0.07 s. By the stress optical rule [13] this plateau level is related to the normal stresses (N1 + N2). After the shear pulse, the flow stresses relax but crystalline orientation becomes visible within a few seconds. Note that the gaps which appear in the figures of our measurement correspond to a pause of 2 s used to write the data to the hard disk between measurement periods of 10 s in our data acquisition system.

Converting these results to birefringence (counting multiples of $\pi/2$ at each extremum of the original curve) we obtain the curve in Figure 2b. It strikingly illustrates how small the orientation is during the shear flow compared to the ensuing orientation during the crystallization.

Flow Birefringence. Kumaraswamy et al.[2,3] pointed out the existence of an unusual upturn in the flow birefringence curve during shear flow and a birefringence which does not relax. They attributed this maximum to the formation of a "shear-induced structure" related to the presence of oriented precursors. The presence of crystalline order during shear was explicitly confirmed using WAXS.[3] We confirm here (Figure 3) the presence of this upturn above 800 s^{-1} in our homogeneously sheared samples. Our data suggest that the upturn arises at lower strains if the strain rate is increased, in agreement with previous observations,[1−3] but since we do not observe a well-defined steady state before the upturn a quantitative determination of a scaling relation for a typical strain does not seem appropriate.

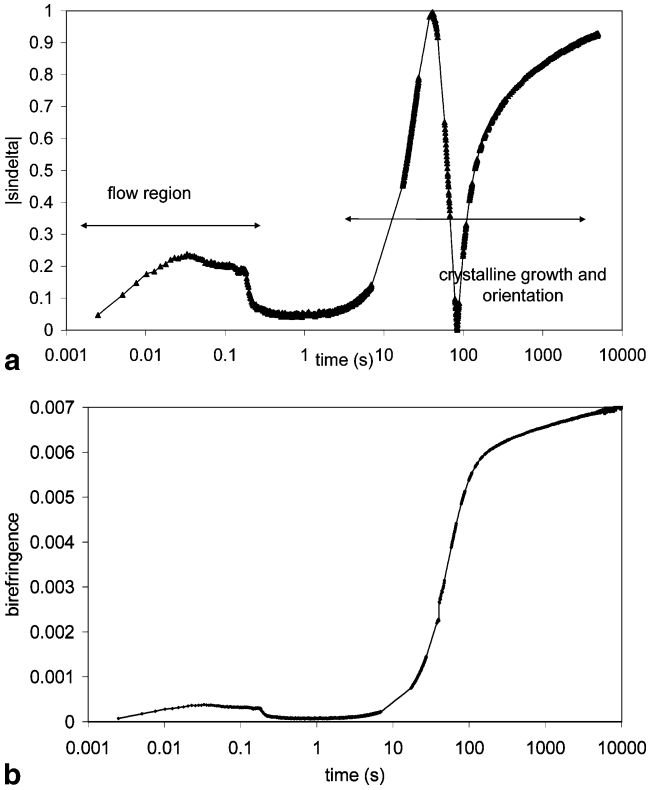

Figure 2. (a) Typical birefringence measurement including flow birefringence and developing crystallization. (b) Birefringence development after a shear pulse.

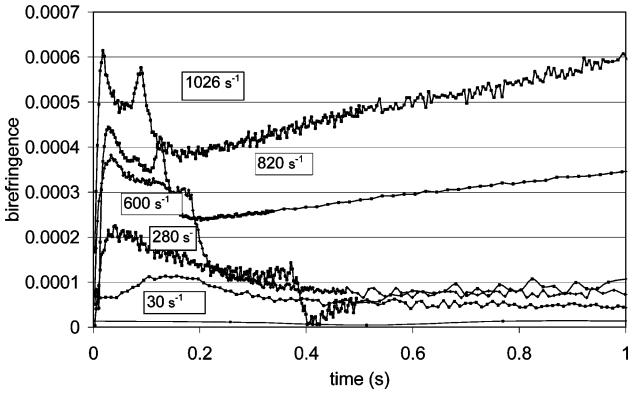

Figure 3. Example of flow birefringence curves measured during shear pulse. The same nominal shear (∼100 shear units) was applied in all experiments.

It is interesting to compare our results to the experimental range obtained in the experiments of Kosher,[4] who examined the crystallization of this same PP in a Linkam shear cell up to a maximum of 50 s^{-1}. Remark that more than a 10-fold increase in shear rate is necessary to reach the strongly oriented region.

Orientation Development after Shear. Even if the first crystallites are sometimes visible within a time span of 0.1 s, much longer times are needed to complete the crystallization. Figure 4 shows typical results obtained by varying the shear rate over 3 orders of magnitude. We recall from the low shear measurements in[4] that a deviation from the quiescent crystallization behavior is already observed above 1 s^{-1}. Considering as crystallization time the one corresponding to the rapid increase in the birefringence curve, a typical time of 20 s is obtained at 1000 s^{-1}, a reduction of a factor of 1000 with respect to quiescent conditions.

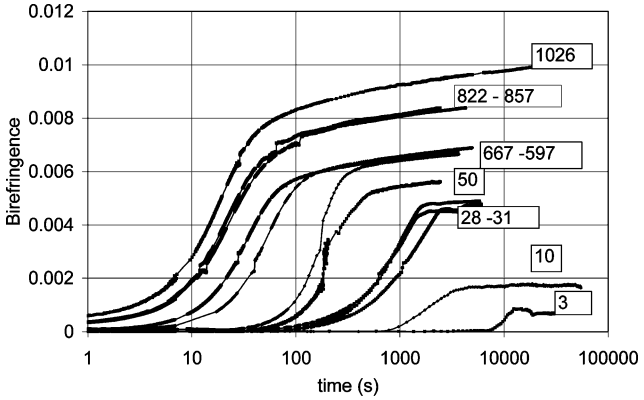

Figure 4. Birefringence development after shear pulse at 140 °C (shear rates are specified).

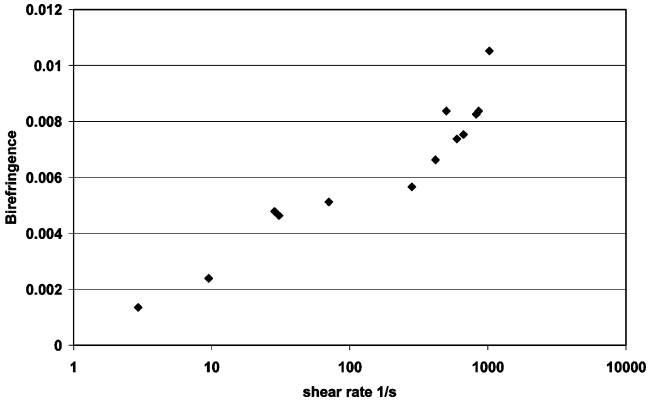

Figure 5. Total birefringence developed in the polypropylene film after shear crystallization at 140 °C.

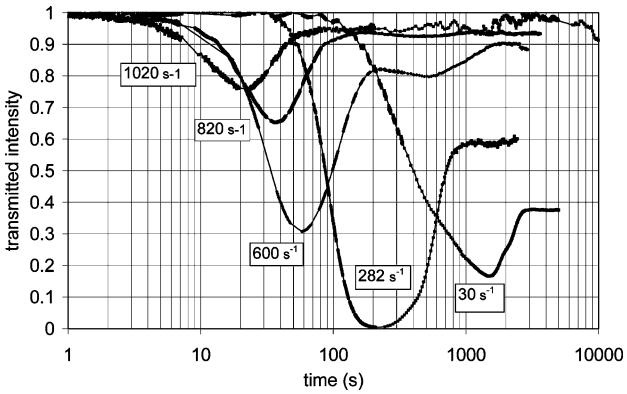

Figure 6. Transmitted intensity as a function of time for different shear rates.

An interesting feature of the above curves is that at the highest rates with a signature from the shear induced structure we also have the more pronounced secondary crystallization mechanism. Our interpretation is that the overall orientation is so dominant that any process that tends to improve the existing lamella or to add lamella by an insertion mechanism can only reinforce this orientation. At lower shear rates, where the structure is spherulitic, the secondary process will mainly add an isotropic component which does not affect the birefringence.

The initial evolution of retardation with time has been discussed[14] with respect to growth speed enhancement during shear and gradual decrease to quiescent growth rates. At the highest shear rates, after substantial crystallization during shear we have a very low slope (even below slope 1). At lower shear rates the slope becomes close to quadratic. A zoom of this region has been provided in the Supporting Information.

The time scale to reach a certain level of retardation has sometimes been used as a measure of the crystallization time. Figure 4 can help us to put this definition into perspective. This definition corresponds to the intersection of the birefringence curves with a horizontal axis with an ordinate depending on the experimental setup. A time corresponding to 50% of the initial rapid increase would probably be a much better definition.

Since we have homogeneous samples and a good control of the sample thickness, we are in a good position to discuss the absolute values of birefringence. As a first approach we compare our data to the level in the mixing law proposed by Samuels[15] for an isotactic PP

$$\Delta_T = \beta\Delta_c{}^0 f_c + (1-\beta)\Delta_{am}{}^0 f_{am}$$

in terms of crystalline volume fraction β, the Herman's orientation factor for crystalline and amorphous regions and the intrinsic birefringence for crystalline and amorphous parts: $\Delta_c{}^0 = 2.91 \times 10^{-2}$, $\Delta_{am}{}^0 = 6.0 \times 10^{-2}$. Birefringence values up to 2.5×10^{-2} in stretched films are reported in the same reference. The final birefringence values that we obtained in our experiments (Figure 5) are much lower: $\Delta \sim 0.01$. We think that these final birefringence values are mainly correlated to the crystalline orientation factor f_c with a crystalline volume fraction β which is located somewhere between 0.6 and 0.7 and only a very weak amorphous contribution. Our birefringence values seem to saturate above 100 s^{-1} at a value of 0.006, but a strong increase is again observable in the high shear rate region, where the oriented shish kebab structure sets in. An attempt at interpretation in terms of a mixing law with orientation factors seems useful because the samples from our shear cell can be easily recovered after crystallization and mechanically tested. We recall that Young's modulus is usually described by a similar mixing law. A further study of the structure−property relations in our samples could be one direction of future work and lead to a better understanding of microstructural behavior in injection molded parts.

It is also tempting to interpret the absolute value of the upturn in birefringence using the two phase model. If, as in ref 14, a 2D model is assumed for radial growth within a cylindrical region having a radius of 100 nm (for an inter-shish distance of 200 nm), a perfect shish ($f_{am} = 1$) of 8 nm diameter can generate an upturn in birefringence of $6 \times 10^{-2}(4/100)^2 \sim 10^{-4}$, as observed. If the shish is much smaller or less perfect and the signal comes from the kebab outgrowth which is the point of view in ref 14, our measurements would indicate that a serious enhancement of radial growth speed is necessary to achieve this. A quiescent growth rate[4] $G = 1.4 \times 10^{-8}$ m/s yields at most a kebab-like outgrowth of 1 nm during the short pulse of 0.1s, whereas at least 7 nm would be necessary to generate the upturn: $0.7(2.9 \times 10^{-2})(7/100)^2 \sim 10^{-4}$. In this estimate, we used a crystalline volume fraction $\beta = 0.7$ within the kebab outgrowth.

Transmitted Intensity. Figure 6 shows the transmitted intensity (IDC, normalized with respect to its initial value) as a function of time. We have three main observations:

- The curves possess a pronounced minimum.
- The intensity of the minimum depends on shear rate.
- At high rates there is almost no loss in intensity, and we obtain highly transparent samples.

That there is an intensity minimum in crystallizing samples has been reported since the first observations in the works of Stein et al.[16] They pointed out the influence of the experimental setup, especially of the opening angle of the detector due to

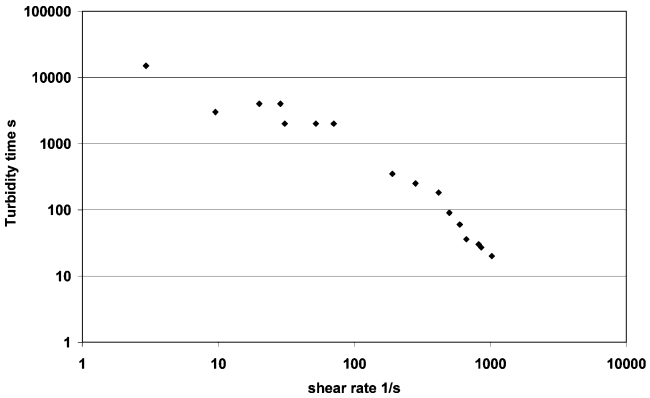

Figure 7. Position of intensity minimum as a function of shear rate.

enhanced forward scattering of larger particles. To quantify the effect they also invoked a Prins-Zernike like theory, but this interpretation seems unlikely since the effect is also present with an incoherent light source. Spruiell and Ding[17] attributed the effect, which is very prominent also during crystallization at higher cooling rates, to impingement which seems a more likely explanation since the impinging structures lose their optical contrast and hence their ability to scatter light. We are not aware of a better theoretical treatment of this phenomenon. The presence of the minimum and its precise location is interesting and a more precise theoretical criterion for what is loosely called "impingement" might provide extra information on the developing morphology. If we assume for instance that the growth rate is constant (a hypothesis that can certainly be improved by interpretation of the slopes of the birefringence curves) and that growth centers are randomly located, a theoretical expression for the scattering power as a function of optical contrast and the number and volume of the scatterers could provide a sound estimate of the number of nuclei.

If the intensity drops to zero, the measurement of birefringence becomes impossible. This is not always dramatic if the time interval where the signal drops below the sensitivity limit of the photodetector is not too long and does not include several oscillations since the birefringence signal can be picked up again after the minimum.

Extrusion die setups inevitably suffer from this effect. Measurements shown in ref 2 exhibit a strongly decreasing intensity which results from a complex superposition of different layers and which completely obscures the birefringence measurement. Our results also show that the use of turbidity half times (moment when the intensity drops to half of its initial value) for the crystallization time scale does not really make sense for high rates since the intensity does not necessarily drop to 50% of its initial value.

Since we believe the minimum to be physically significant, we found it instructive to plot a turbidity time (defined by the position of the minimum) in Figure 7. At the lowest shear rates, the presence of a minimum is questionable, but since the size of the laser spot becomes in that case comparable to the size of the spherulites, this type of setup is not the most appropriate to measure crystallization kinetics. Figure 7 clearly illustrates a

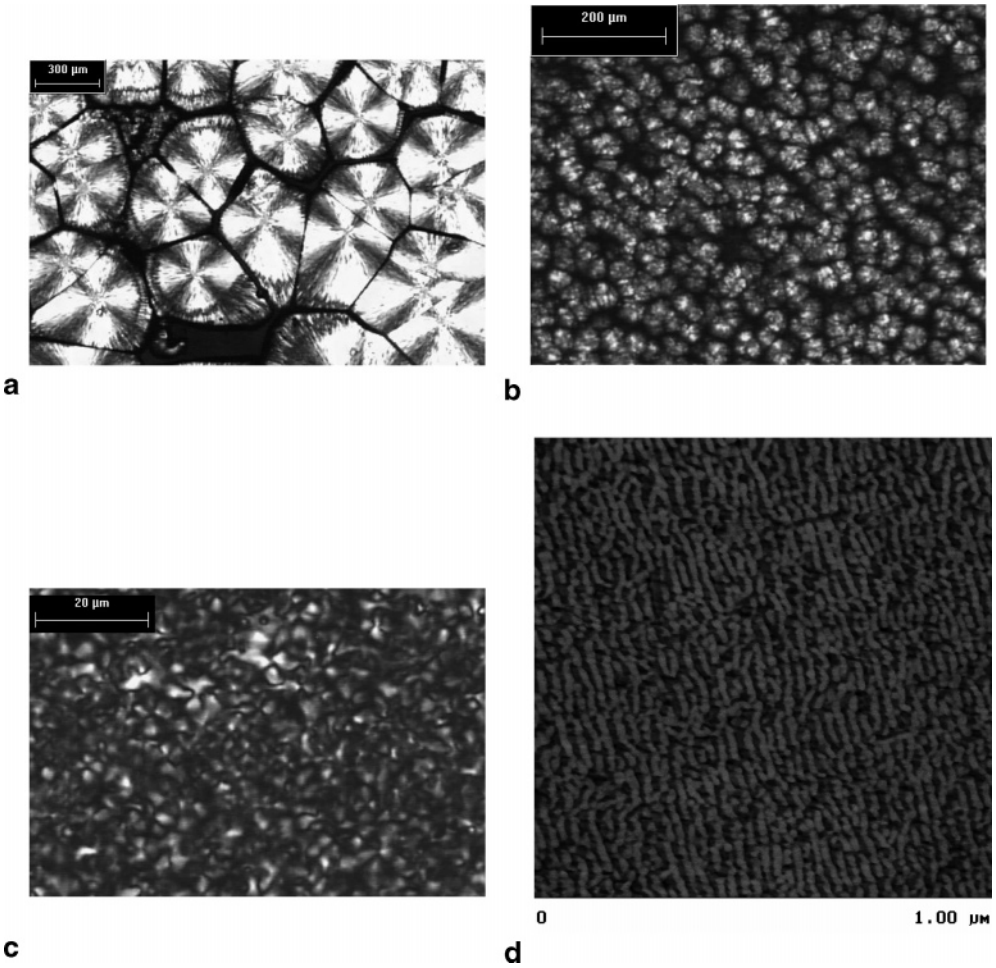

Figure 8. (a) Morphology after quiescent crystallization: 300 μm spherulites. (b) Morphology after a shear pulse of 30 s^{-1} (110 shear units): 40 μm spherulites. (c) Morphology after a shear pulse at 300 s^{-1} (110 shear units): 4 μm spherulites. (d) AFM image of morphology after shear at 1000 s^{-1} (100 shear units). The flow direction is almost horizontal perpendicular to the lamellae.

change in slope at the highest shear rates accompanying the unusual upturn in the birefringence curve. At high rate this turbidity time is seen to scale as $\dot{\gamma}^{-2}$.

Morphology. Examination of the morphology on the obtained films shows large 300 μm spherulites after quiescent crystallization in Figure 8a. Increasing the shear rate while maintaining the imposed shear close to 100 shear units we obtain 40 μm sized spherulites at 30 s^{-1} (Figure 8b) and 4 μm sized structures at 300 s^{-1} (Figure 8c). At high shear rates, the structure looks completely transparent and structureless according to optical microscopy. Using AFM (Figure 8d) a uniform row nucleated structure appears with relatively short (<100 nm) and parallel lamellae.

TEM images that are not reproduced here show the presence of very thin "shish" spaced about 200 nm apart. These TEM images are very similar to those of Seki.[18] Some of the AFM images also suggest the presence of zones emanating from a center line.

Limits. At the highest shear rates examined for this product (1000 s^{-1}), we find more scattering in our experimental results which indicate that we get closer to an experimental limit or an instability. Above the highest shear rates used in our graphs the experiments fail as the samples get inhomogeneous and exihibit zones with distinct morphology along the flow direction which we interpret as stick−slip zones. We think that the polymer loses adhesion to the glass wall, thereby locally promoting an elongational flow. In these zones, we observe a fine fibrous structure. If one of these fibers happens to be intercepted by the laser beam, much higher levels of birefringence are observed than the ones reported here, starting already during the shear pulse. It is of course possible that the loss of adherence is provoked by the crystallization during the shear pulse, but this might be difficult to prove.

4. Conclusions

Thanks to the construction of a new sandwich type shear cell enabling us to operate up to 1000 s^{-1} and the use of a modulated laser, we have been able to present a global view of shear-induced orientation in an isotactic PP sample at 140 °C. The new cell provides homogeneously sheared samples starting from the low shear rates where we only see nucleation enhancement up to the highest rates with a columnar morphology that is templated by precursors. Remarkable is the gradual rise of anisotropy in the samples despite the maintenance of the spherulitic geometry. At higher rates, this is followed by a much sharper rise in birefringence and we confirm the observations in ref 2 that this occurs together with the characteristic upturn in the flow birefringence pattern. We believe to be the first to present birefringence values throughout the complete transition, and we have presented it here for one level of shear and one temperature. Further work will be done to examine the effect of these other parameters. Remarkable also is the characteristic evolution of transmitted intensity with a characteristic minimum. We propose to study more in detail this characteristic minimum to get a better characterization of the crystallization process using optical techniques.

Acknowledgment. We acknowledge discussions on the OAM setup with P. Venema at Wageningen University and on optical instrumentation with S. Blanc. Thanks to E. Overtus, T. Wilot, and F. Vilaine for engineering and experimental support and to C. Dehennau for supporting the project. We also acknowledge financial support of the Région Bruxelloise (IRSIB project).

Supporting Information Available: Text discussing the rheological characterization of the used PP and slopes of the birefringence curves, figures showing rheological behaviour of PP-A, the linear viscoelastic behaviour, and birefringence development for different shear rates, and a table of the explicit viscoelastic data. This material is available free of charge via the Internet at http://pubs.acs.org.

References and Notes

(1) Eder, G.; Janeschitz-Kriegl, H. In *Processing of Polymers*; Meijer, H. E. H., Ed.; VCH: New York, 1997; Vol. 18, Chapter 5.
(2) Kumaraswamy, G.; Issaian, A.; Kornfield, J. A. *Macromolecules* **1999**, *32*, 7537−7547.
(3) Kumaraswamy, G.; Verma, R. K.; Issaian, A.; Wang, P.; Kornfield, J. A.; Yeh, F.; Hsiao, B. S.; Olley, R. H. *Polymer* **2000**, *41*, 8931−8940.
(4) Koscher, E.; Fulchiron, R. *Polymer* **2002**, *43*, 6931−6942.
(5) Devaux, N.; Monasse, B.; Haudin, J. M.; Moldenaers, P.; Vermant, J. *Rheol. Acta* **2004**, *43*, 210−222.
(6) Janeschitz-Kriegl, H.; Ratajski, E. *Polymer* **2005**, *46*, 3856−3870.
(7) Doufas, A. K.; Mc. Hugh, A. J.; Miller, C. *J. Non-Newtonian Fluid Mech.* **2000**, *92*, 27−66.
(8) Zuidema, H. Ph.D. Thesis, T. U. Eindhoven **2000**.
(9) Zheng, R.; Kennedy, P. *J. Rheol.* **2004**, *48*, 823−842.
(10) Fuller, G. G. *Optical Rheometry of Complex Fluids*; Oxford University Press: New York, 1995.
(11) Lagasse, R. R.; Maxwell, B. *Polym. Eng. Sci.* **1976**, *16*, 189−199.
(12) Van Meerveld, J.; Peters, G. W. M.; Hütter, M. *Rheol. Acta* **2004**, *44*, 119−134.
(13) Janeschitz-Kriegl, H. *Polymer Melt Rheology and Flow Birefringence*; Springer-Verlag: Berlin, 1983.
(14) Kumaraswamy, G.; Verma, R. K.; Issaian, A.; Wang, P.; Kornfield, J. A.; Yeh, F.; Hsiao, B. S. *Macromolecules* **2004**, *37*, 9005−9017.
(15) Samuels R. J. *Structured Polymer Properties*; Wiley-Interscience: New York, 1974.
(16) Clough, S.; Rhodes, M. B.; Stein, R. S. *J. Polym. Sci. C* **1967**, *18*, 1−32.
(17) Ding, Z.; Spruiell, J. E. *J. Polym. Sci. B* **1996**, *34*, 2783−2804.
(18) Seki, M.; Thurman, D. W.; Oberhauser, J. P.; Kornfield, J. A. *Macromolecules* **2002**, *35*, 2583−2594.

MA0525684